



Improved Capacity of $\text{LiNi}_{0.8}\text{Mn}_{0.1}\text{Co}_{0.1}\text{O}_2$ Cathode upon Sn(IV) Doping by Facile Co-Precipitation Method

D. DEIVAMANI and P. PERUMAL*

P.G. and Research Department of Physics, Alagappa Government Arts College, Karaikudi-630003, India

*Corresponding author: E-mail: perumal59@gmail.com

Received: 22 November 2019;

Accepted: 28 December 2019;

Published online: 30 May 2020;

AJC-19874

Nickel rich lithium nickel manganese cobalt oxide is one of the prominent cathode materials in the field of lithium ion battery. The cathode was prepared upon doping with Sn^{4+} by simple co-precipitation method to develop its discharge capacity. The structural and morphological studies on the cathode material were done by X-ray diffraction and scanning electron microscopy to confirm any structural changes upon doping of Sn^{4+} . The higher discharge capacity of 210 mAh g^{-1} with 89% capacity retention was achieved even after 100 cycles at C/3 rate for 0.8 mol % Sn^{4+} doped lithium nickel manganese cobalt oxide. The structural phase change upon cycling for Sn^{4+} doped and un-doped cathode was illustrated by differential plot. The ionic radius and high bond stability of Sn^{4+} that compares Ni^{2+} might be the reason to prevent structural collapse during Li^+ intercalation and de-intercalation process.

Keywords: Cathode material, Co-precipitation method, Tin(IV), Doping, Lithium ion battery.

INTRODUCTION

A field of application of lithium ion batteries has been growing rapidly since the commercialization of lithium cobalt oxide as cathode material in 1991 by Sony Corporation, Japan [1-6]. It is being used in several consumer electronics because of its higher energy density comparing to other secondary batteries. Researchers have been focusing their attention to improve the capacity, performance and safety of lithium ion batteries due to its big potential market especially in the development of electric vehicle [2,7]. Lithium cobalt oxide possesses high energy density that making it an ideal choice for small devices. Electrical propulsion requires cathode materials that supplies higher capacity to satisfy demands of $\sim 500 \text{ km}$ /charge driving range and long life. In the development of cathode for lithium ion battery, the lithium cobalt oxide was the first material to investigate as a intercalation compound with Li ion, thereafter the identification of different intercalation materials paved way to diverse its path in different angles. Numbingly, the most common lithium ion intercalating members are Spinel- LiMn_2O_4 [1-3] and olivine- LiFePO_4 (LFP) [4,5]. The substitution of Mn in the spinel system with Ni also considered as a

stable cathode material with higher operating potential up to 5 V. This $\text{LiMn}_{1.5}\text{Ni}_{0.5}\text{O}_4$ [6,7] is one of the prominent material and been used in the commercial application as well by number of cell makers. The material called zero strain material is LFP, which will cycle more thousands number of cycles without any capacity decay. The major drawback of this material is low conductivity of the order of 10^{-6} Scm^{-2} [8-11]. This conductivity issue has been tackled by coating the material with conductive carbon additives. Moreover, nanosized LFP would be more preferred to improvise the conductivity and Li^+ diffusion over the solid matrix. On the other hand, carbon coating and high surface area exerted by nanomaterials brought down the material density than other family of common cathode material. So, collectively LFP is having drawback in its lesser volumetric density and energy density. As far as spinel material is concerned the Jahn-Teller distortion [3,12-14] and Mn ion dissolution at lower potential caused large capacity loss over cycles. Also, Mn ion deposition on the anode plays a significant role in capacity fade. Hence, in the family of layer crystal structured there are individual candidates like LiCoO_2 , LiMnO_2 [15] and LiNiO_2 [16,17], which exhibited the intercalation properties with Li^+ , but all these candidates suffered with structural insta-

bility over the period of cycling [8-10]. The different combinations of consisting binary, tertiary and quaternary lithium metal oxide systems having layered geometry exhibits different number in capacity and performance. But, each of them are having different issues which could not serve the purpose as a prominent candidate for long term and high rate applications [18-20]. Nevertheless, mixed transition metal oxide cathode material consisting most commonly Ni, Mn, Co and Al having the general nomenclature of NCA ($\text{LiNi}_{1-x-y}\text{Co}_x\text{Al}_y\text{O}_2$, $\text{Ni} = \sim 0.9$ and $\text{Al} = 0.05$) [11-14] and NCM/NMC ($\text{LiNi}_{1-x-y}\text{Co}_x\text{Mn}_y\text{O}_2$, $\text{Ni} = 0.3$ to 0.9) [15-18] based on the use of utilization of Al and Mn, respectively. Significantly, a development of NMC has started from well-known composition of $\text{LiNi}_{1/3}\text{Co}_{1/3}\text{Mn}_{1/3}\text{O}_2$ and now the researchers are working on LiNiO_2 (LNO) [19-23] which would replace all other transition metals with Ni to stabilize the structural stability and to improve high temperature stability especially at higher charge voltage above 4.2 V. Importantly, a well-established composition of NMC family is $\text{LiNi}_{0.8}\text{Mn}_{0.1}\text{Co}_{0.1}\text{O}_2$ (NMC811) and working on this composition of NMC811 worth more to bring this material for commercialization process. Therefore, NMC811 has been studied extensively by researchers which deliver the capacity of ~ 200 mAh g^{-1} [24,25]. The major drawback of these material is the poor stability during prolong charge-discharge cycles. The capacity fading is also directly correlated with Ni content of the material, *i.e.* higher the Ni content, lower the capacity retention. The occurrence of cracking at the surface of this material during charging at higher potential above 4.1 V was due to large cell volume change upon lithium intercalation [26]. In addition, a carbonate electrolyte intervention at the surface influences the oxidation of O^{2-} and produces O_2 gas. Consequently, the formation of rock salt kind structure takes place due to the migration of Ni from its transition metals octahedral site to Li layer that leads to building up of impedance over cycling [26-29].

Moreover, a tradition of using a trace amount of foreign metal cations in the parent composition had been impacted in the performance of the material especially in lithium ion batteries cathode materials. Many reports have been enroute to overcome these issues by modifying or protecting the surface to minimize the parasitic reaction due to the electrolytic species and also the method of doping in to the transition metal layer with suitable metal ions to reduce the volume expansion during charge-discharge process [9,19,30-34]. The volume change of crystal structure along the perpendicular axis during charge-discharge specifically above 4.1 V due to H3 phase formation generally occurs for the high Ni cathode system in lithium ion batteries. Therefore, a relatively similar sized Sn^{4+} which shows ionic radius equivalent to Ni^{2+} was used to study NMC811 as one of the dopant, also, the effect of Sn in lithium nickel manganese cobalt oxide cathode material has been reported earlier [35-37]. In present work, an effect of doping of Sn^{4+} on the capacity and cycling performance of NMC811 has been studied with the more facile method of solid-state annealing method in a controlled manner which is described henceforth. Hence, this work revealed the structural and electrochemical correlation for the improved effect of Sn^{4+} cation on stabilizing the transition metal octahedral geometry in the crystal [35,38].

EXPERIMENTAL

The undoped NMC811 cathode material and 0.8 mol% and 1.0 mol% Sn doped NMC811 were prepared by facile co-precipitation method. The nickel sulfate, manganese sulfate and cobalt sulfate were used as procured to carry out the reaction. All the chemicals used in this work were of analytical grade (99.99% purity, Sigma-Aldrich). A 5N NaOH solution and 0.5M NH_4OH mixture were taken in a separate flask and its flow was controlled by a stopper. The separate flask was used to dissolve required stoichiometric amount of mixture of transition metal sulphate salts (3N). The flow of transition metal salts mix was fixed at 50 mL/min and flow of base solution was monitored to have pH 11 and collected in the reaction vessel. The reaction vessel was stirred to maximum speed of 800 rpm at constant temperature 50 °C. The same process was carried out for Sn doped NMC811 by adjusting tin(IV) sulphate concentration to get 1 and 0.8 mol% doped NMC811. The precipitate hydroxide precursors was filtered and collected separately and then the sample were washed and dried at 105 °C. The 1.03 mol% equivalent amount of $\text{LiOH}\cdot\text{H}_2\text{O}$ salt was mixed with hydroxide precursor in a gentle manner with mortar and pestle. The precursor have annealed at box furnace at 800 °C with high pure oxygen flow at a controlled rate of 0.5 L/min. The furnace was left to cool down to room temperature with the oxygen flow. The final product were collected and characterized to realize its applications in lithium ion batteries as cathode materials.

Powder X-ray diffraction pattern were recorded to elucidate its crystal nature using BRUKER in the 2θ range 10-80° and step 0.02. The morphology of samples was analyzed by using JOEL JSM 840 Scanning Electron Microscopy (SEM). CR-2032 type coin cells were used to fabricate 2-electrode half-cell consisting active material as working electrodes and Li metal as anode and reference electrodes. The working electrode were prepared by taking 80% active materials, 10% conductivity carbon black and 10% PVDF binder. A 1M LiPF_6 in 1:1 EC:DEC solution were used as electrolyte. The ionically conductive single layer polypropylene was used as separator. The galvanostatic and potentiostatic cycling was measure using BIOLOGIC BCS-810 system.

RESULTS AND DISCUSSION

X-ray diffraction studies: Fig. 1 shows the X-ray diffraction patterns of undoped and Sn^{4+} doped NMC811 cathode materials. The crystal lattice parameters and cell volume have been calculated by X'pert highscore plus. From Fig. 1, X-ray diffraction pattern of Sn^{4+} doped and undoped NMC811 are well matched with the layered α - NaFeO_2 type crystal structure with the space group R-3m, which is primarily evident for the formation of the layered structure. From Table-1, the lattice parameters and cell volumes of doped NMC811 showed a little variation than undoped NMC811. Similar kind of results was also reported by many researchers [11,16-18]. The lattice parameter along *c*-axis which was corresponds to the (0 0 3) plane show little shift between undoped and doped samples (Table-1). The *c/a* value was also found about ~ 4.94 for all the samples. Hence, the 'a', 'c' values typically exhibits the characteristic values for the layered NMC811 kind of cathode materials. The peak

TABLE-1
X-RAY DIFFRACTION PATTERN DERIVED DATA OF UNIT CELL PARAMETERS, CELL VOLUME AND I_{003}/I_{104} INTENSITY RATIO VALUES FOR THE UNDOPED AND Sn^{4+} DOPED NMC811 CATHODE MATERIAL

Material	a (Å)	b (Å)	c/a	Volume (Å ³)	I_{003}/I_{104}
NMC811	2.8714	14.2057	4.9473	101.4387	1.77
0.8 mol% Sn	2.8727	14.2082	4.9459	101.5430	1.73
1.0 mol% Sn	2.8709	14.2068	4.9486	101.5635	1.77

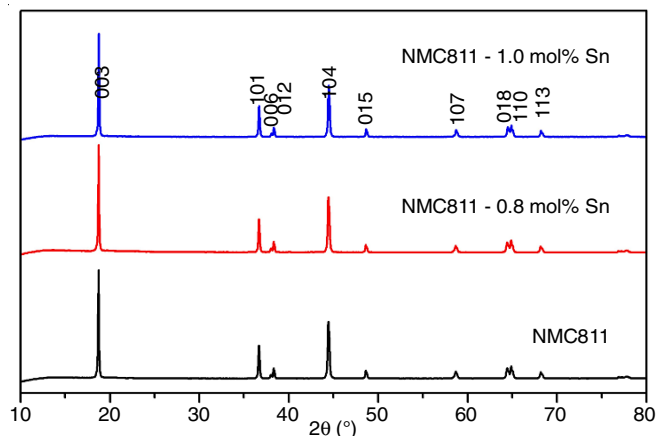


Fig. 1. X-ray diffraction pattern of the un-doped NMC811 and 0.8 mol% and 1.0 mol% Sn^{4+} doped NMC811 after annealing at 800 °C under oxygen atmosphere

intensity ratio I_{003}/I_{104} showed the value above 1.2 signifies the ordering of lithium and transition metal layer structure. Hence, a superior performance of Sn^{4+} was might be due to the occupation of Sn^{4+} cation (ionic radii 0.55 a.u.) in the place of Ni^{3+}

(ionic radii 0.56 a.u.)/ Ni^{2+} (ionic radii 0.55 a.u.) of the MO_6 layer. Consequently, Sn^{4+} doping did not altered the crystal structure of NMC811 due to its similarity in ionic radii. At the same time, an amount of dopant having higher oxidation state (Sn^{4+}) prevent the formation of Ni^{3+} from Ni^{2+} and the resulting in little higher capacity by Ni^{2+} to Ni^{4+} transition while delithiation [39]. Thus, a ratio of $\text{Ni}^{2+}/\text{Ni}^{3+}$ is higher in the case of Sn^{4+} doped NMC811 than the undoped.

SEM studies: The surface morphologies of undoped and Sn^{4+} doped hydroxide precursors prepared *via* co-precipitation method is shown in the Fig. 2a-c. Also, the SEM images of the same undoped and Sn^{4+} doped NMC811 materials after lithiation by the annealing process at 800 °C under oxygen ambient are shown in Fig. 2d-f. Fig. 2a and 2d illustrates the morphology of undoped NMC811 hydroxide precursor and lithiated NMC811 material respectively. whereas Fig. 2b and 2c (hydroxide pre-cursor), 2e and 2f showed 0.8 and 1.0 mol% Sn^{4+} doped NMC811, respectively. It was observed that an image of precursors showed a aggregates of small particles while on the contrary well separated secondary particles with size ranging from 5 to 20 μm were noticed for the samples

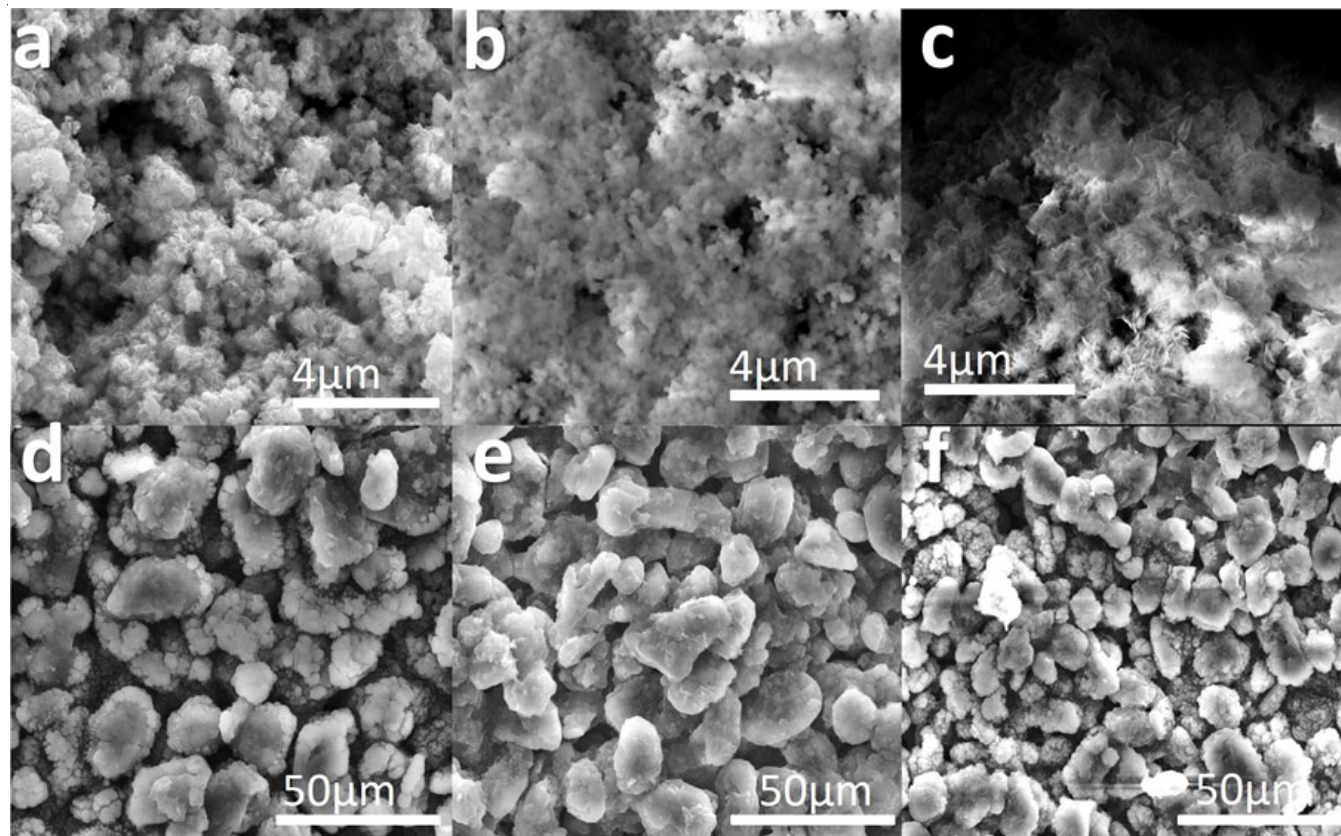


Fig. 2. Scanning electron microscopic images of (a) undoped NMC811 (b) 0.8 mol% Sn^{4+} doped NMC811 (c) 1.0 mol% Sn^{4+} doped NMC811 hydroxide precursors and (d) undoped NMC811 (e) 0.8 mol% Sn^{4+} doped NMC811 (f) 1.0 mol% Sn^{4+} doped NMC811 after annealing at 800 °C under oxygen atmosphere

annealed at 800 °C. From Fig. 2e, 0.8 mol% Sn⁴⁺ doped NMC811 showed a smooth uniform agglomerated particle than other samples. As uniformity increases, the total gap density of 0.8 mol% Sn⁴⁺ doped NMC811 also increases that helps in higher material loading and consequently increases the energy density of the cell.

Electrochemical performance: The undoped and doped NMC811 cathode materials are subjected to charge-discharge cycling test at C/3 rate for 100 cycles in order to understand the effect of Sn⁴⁺ doping (Fig. 3a). The undoped NMC811 exhibited a discharge capacity of around 175 mAh g⁻¹ for the 1st cycle and 130 mAh g⁻¹ for the 100th cycle at C/3 rate which was lesser than Sn⁴⁺ doped NMC811. The cathodes 0.8 mol% and 1 mol% Sn⁴⁺ doped NMC811 delivered the discharge capacity of 210 and 200 mAh g⁻¹ for the first cycle, respectively and correspondingly the capacity retention data exhibits for the studied 100 cycles that doped material have established a significant contribution than undoped NMC811. Fig. 3b shows the charge-discharge cycling performance of undoped and doped cathodes at different C-rates. The 0.8 mol% Sn⁴⁺ doped NMC811 delivered a higher discharge capacity than undoped NMC811 for all C-rate ranging from 0.1C to 0.8C. Fig. 4a shows a charge-discharge curve of the cell 0.8 mol% Sn doped NMC811 cycled between 2.8 to 4.3 V of 1st, 40th, 80th and 100th cycle.

Fig. 3 represents a discharge capacity against cycle number, which signified that 0.8 mol% Sn⁴⁺ doped NMC811 shows a

higher discharge capacity than undoped and 1 mol% Sn⁴⁺ doped NMC811. This was due to the surface smoothness and uniformity of the particles. The capacity was found to be reduced at higher concentration of dopant and due to reduction in number of available redox couple Ni^{2+/3+} to Ni⁴⁺ during charge-discharge. A well-known surface cracking phenomenon for the higher nickel content in NMC cathode is due to the interference of electrolyte decomposition and oxygen evolution at the surface over prolonged charge-discharge cycles, which causes the loss of capacity [19,28,40-42]. The dopant Sn⁴⁺ lessens the above effect and stabilizes O-M-O octahedral geometry of transition metal layer of the crystal lattice during the intercalation and de-intercalation process. Hence, a doping of Sn cation shows an intense effect in preventing the crystal structure during charging-discharging and also helps to improve the capacity [35,38, 43]. The charge-discharge curve in Fig. 4a explains the profile of constant current-constant voltage charge (CC-CV) and constant current discharge for 0.8 mol% doped material. Evidently from Fig. 3c, the average voltage plot for the charge-discharge cycles until 100 cycles revealed and promotionally supports for the better performance of 0.8 mol% Sn⁴⁺ doped NMC811 than undoped one. In addition, it was also noticed from Fig. 4b that the formation of characteristic H3 phase, observed at 4.2 V for nickel rich cathode, which educates about the additional higher capacity while comparing other materials of having Ni lower than 80% of transition metal of NMC families. Significantly,

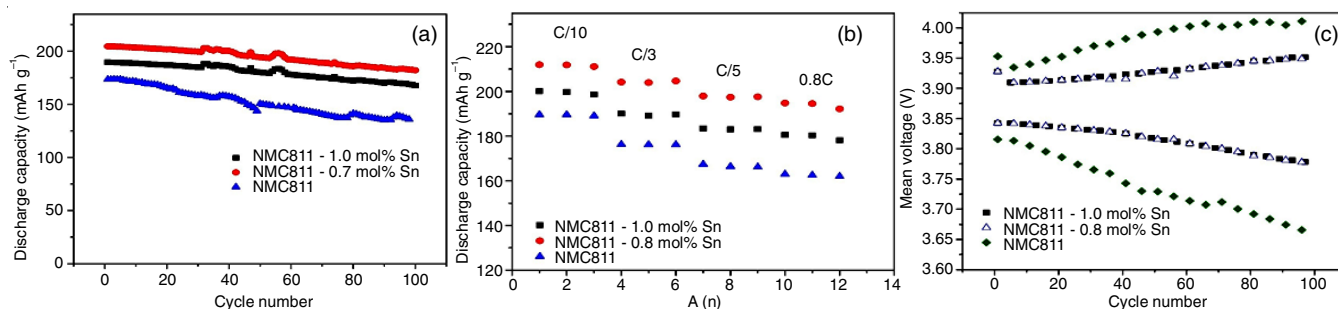


Fig. 3. (a) Discharge capacity of undoped NMC811, 0.8 mol% and 1.0 mol% Sn⁴⁺ doped NMC811 for 100 cycles at C/3 rate (b) Discharge capacity against different C-rate (c) Mean charging-discharging plateau voltage corresponding to each cycles

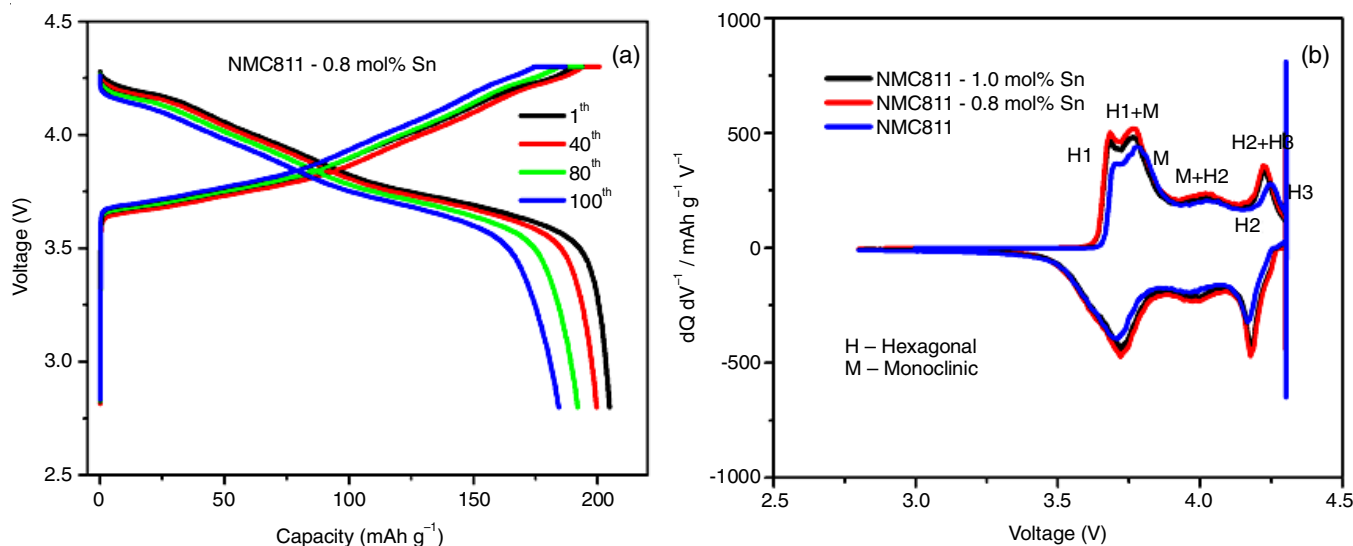


Fig. 4. (a) 1st, 40th, 80th and 100th cycle charge-discharge profile of 0.8 mol% doped NMC811 material cycled between 2.8 to 4.3 V in CC-CV charge CC discharge mode. (b) Differential capacity (dQ/dV) with respect to voltage for the 0.8 mol% Sn⁴⁺ doped NMC811

the phase shift and higher polarization could be seen from the undoped NMC811 cathode material, which causes the higher voltage hysteresis and poor performance [44,45]. The differential capacity plot (dQ/dV) against voltage (V) was derived for undoped and Sn⁴⁺ doped NMC811 and is shown in Fig. 4b. The dQ/dV versus V plot exhibited a typical phase change behaviour for the Ni-rich NMC material [44,45]. The volume change along the *c*-axis during charge-discharge would lead to the irreversibility in the H3 to H2 phase and consequently forms rock salt spinel nickel oxide. The phase reversibility has been improved upon doping of Sn⁴⁺ might be due to the reduction in the volume change during charge-discharge process.

Conclusion

The undoped NMC811 and Sn⁴⁺ doped NMC811 cathode material were prepared by co-precipitation and post-lithiation process. X-ray diffraction pattern confirmed that the presence of Sn⁴⁺ in the crystal lattice and have not shown any impurity peak and hence Sn⁴⁺ did not alter the structure of NMC811. SEM morphologies inferred that the doping process involving annealing has no influence on the morphology. The electrochemical charge-discharge studies revealed that 0.8 mol% Sn⁴⁺ doped NMC811 provides desirable high capacity while maintains retention. The average voltage during discharging cycles evidence the comparative improvement of Sn⁴⁺ doping with undoped NMC811. The phase change was occurred for the Ni-rich NMC material, which was proved from its the fingerprint voltage region. Thus, this work has demonstrated a facile method to improve the capacity and stability of Ni-rich NMC cathode material upon doping of Sn⁴⁺.

ACKNOWLEDGEMENTS

One of the authors, D. Deivamani acknowledges UGC-SERO, Hyderabad, India for granting FDP fellowship for carrying out this research work.

CONFLICT OF INTEREST

The authors declare that there is no conflict of interests regarding the publication of this article.

REFERENCES

- M.S. Whittingham, *Chem. Rev.*, **104**, 4271 (2004); <https://doi.org/10.1021/cr020731c>
- S. Flandrois and B. Simon, *Carbon N.Y.*, **37**, 165 (1999); [https://doi.org/10.1016/S0008-6223\(98\)00290-5](https://doi.org/10.1016/S0008-6223(98)00290-5)
- D. Aurbach, Y. Talyosef, B. Markovsky, E. Markevich, E. Zinigrad, L. Asraf, J.S. Gnanaraj and H.-J. Kim, *Electrochim. Acta*, **50**, 247 (2004); <https://doi.org/10.1016/j.electacta.2004.01.090>
- W. Guo, X. Xue, S. Wang, C. Lin and Z.L. Wang, *Nano Lett.*, **12**, 2520 (2012); <https://doi.org/10.1021/nl3007159>
- W. Lu, J. Liu, Y.K. Sun and K. Amine, *J. Power Sources*, **167**, 212 (2007); <https://doi.org/10.1016/j.jpowsour.2006.12.077>
- X.Z. Liao, Y.S. He, Z.F. Ma, X.M. Zhang and L. Wang, *J. Power Sources*, **174**, 720 (2007); <https://doi.org/10.1016/j.jpowsour.2007.06.146>
- X. Yu, Y. Lyu, L. Gu, H. Wu, S.-M. Bak, Y. Zhou, K. Amine, S.N. Ehrlich, H. Li, K.-W. Nam and X.-Q. Yang, *Adv. Energy Mater.*, **4**, 1300950 (2014); <https://doi.org/10.1002/aenm.201300950>
- T.E. Sutto, *Inorg. Chem.*, **53**, 4570 (2014); <https://doi.org/10.1021/ic500252c>
- C. Tian, F. Lin and M.M. Doeff, *Acc. Chem. Res.*, **51**, 89 (2018); <https://doi.org/10.1021/acs.accounts.7b00520>
- C. Li, H.P. Zhang, L.J. Fu, H. Liu, Y.P. Wu, E. Rahm, R. Holze and H.Q. Wu, *Electrochim. Acta*, **51**, 3872 (2006); <https://doi.org/10.1016/j.electacta.2005.11.015>
- S.K. Martha, B. Markovsky, J. Grinblat, Y. Gofer, O. Haik, E. Zinigrad, D. Aurbach, T. Drenzen, D. Wang, G. Deghenghi and I. Exnar, *J. Electrochem. Soc.*, **156**, A541 (2009); <https://doi.org/10.1149/1.3125765>
- J.-W. Shin and J.-T. Son, *J. Korean Phys. Soc.*, **74**, 53 (2019); <https://doi.org/10.3938/jkps.74.53>
- Z.W. Lebens-Higgins, S. Sallis, N.V. Faenza, F. Badway, N. Pereira, D.M. Halat, M. Wahila, C. Schlueter, T.-L. Lee, W. Yang, C.P. Grey, G.G. Amatucci and L.F.J. Piper, *Chem. Mater.*, **30**, 958 (2018); <https://doi.org/10.1021/acs.chemmater.7b04782>
- H. Winkler, *Arch. Psychiatr. Nervenkr.*, **91**, 495 (1930); <https://doi.org/10.1007/BF01815652>
- B. Han, T. Paulauskas, B. Key, C. Peebles, J.S. Park, R.F. Klie, J.T. Vaughey and F. Dogan, *ACS Appl. Mater. Interfaces*, **9**, 14769 (2017); <https://doi.org/10.1021/acsami.7b00595>
- J. Li, R. Shunmugasundaram, R. Doig and J.R. Dahn, *Chem. Mater.*, **28**, 162 (2016); <https://doi.org/10.1021/acs.chemmater.5b03500>
- S.K. Martha, H. Sclar, Z. Szmuk Framowitz, D. Kovacheva, N. Saliyski, Y. Gofer, P. Sharon, E. Golik, B. Markovsky and D. Aurbach, *J. Power Sources*, **189**, 248 (2009); <https://doi.org/10.1016/j.jpowsour.2008.09.090>
- S.-M. Bak, E. Hu, Y. Zhou, X. Yu, S.D. Senanayake, S.-J. Cho, K.-B. Kim, K.Y. Chung, X.-Q. Yang and K.-W. Nam, *ACS Appl. Mater. Interfaces*, **6**, 22594 (2014); <https://doi.org/10.1021/am506712c>
- C.S. Yoon, H.-H. Ryu, G.-T. Park, J.-H. Kim, K.-H. Kim and Y.-K. Sun, *J. Mater. Chem. A*, **6**, 4126 (2018); <https://doi.org/10.1039/C7TA11346C>
- T. Ohzuku, *J. Electrochem. Soc.*, **140**, 1862 (1993); <https://doi.org/10.1149/1.2220730>
- C.S. Yoon, D.-W. Jun, S.-T. Myung and Y.-K. Sun, *ACS Energy Lett.*, **2**, 1150 (2017); <https://doi.org/10.1021/acseenergylett.7b00304>
- C.S. Yoon, U.-H. Kim, G.-T. Park, S.J. Kim, K.-H. Kim, J. Kim and Y.-K. Sun, *ACS Energy Lett.*, **3**, 1634 (2018); <https://doi.org/10.1021/acseenergylett.8b00805>
- C.S. Yoon, U.-H. Kim, G.-T. Park, S.J. Kim, K.-H. Kim, J. Kim and Y.-K. Sun, *ACS Energy Lett.*, **3**, 1634 (2018); <https://doi.org/10.1021/acseenergylett.8b00805>
- H.-H. Ryu, K.-J. Park, C.S. Yoon and Y.-K. Sun, *Chem. Mater.*, **30**, 1155 (2018); <https://doi.org/10.1021/acs.chemmater.7b05269>
- Project, A.M.Q. Stabilized NMC811 to Enable High Energy Density Lithium Ion Batteries.
- E. Hu, X. Wang, X. Yu and X.-Q. Yang, *Acc. Chem. Res.*, **51**, 290 (2018); <https://doi.org/10.1021/acs.accounts.7b00506>
- P.K. Nayak, J. Grinblat, M. Levi, E. Levi, D. Zitoun, B. Markovsky and D. Aurbach, *Mater. Sci. Eng. B*, **213**, 131 (2016); <https://doi.org/10.1016/j.mseb.2016.04.012>
- S.-K. Jung, H. Gwon, J. Hong, K.-Y. Park, D.-H. Seo, H. Kim, J. Hyun, W. Yang and K. Kang, *Adv. Energy Mater.*, **4**, 1300787 (2014); <https://doi.org/10.1002/aenm.201300787>
- L. Mu, R. Lin, R. Xu, L. Han, S. Xia, D. Sokaras, J.D. Steiner, T.-C. Weng, D. Nordlund, M.M. Doeff, Y. Liu, K. Zhao, H.L. Xin and F. Lin, *Nano Lett.*, **18**, 3241 (2018); <https://doi.org/10.1021/acs.nanolett.8b01036>
- S.J. Do, P. Santhoshkumar, S.H. Kang, K. Prasanna, Y.N. Jo and C.W. Lee, *Ceram. Int.*, **45**, 6972 (2019); <https://doi.org/10.1016/j.ceramint.2018.12.196>
- Y. Kou, E. Han, L.Z. Zhu, L. Liu and Z. Zhang, *Solid State Ion.*, **296**, 154 (2016); <https://doi.org/10.1016/j.ssi.2016.09.020>
- S. Neudeck, F. Walther, T. Bergfeldt, C. Suchomski, M. Rohnke, P. Hartmann, J. Janek and T. Brezesinski, *ACS Appl. Mater. Interfaces*, **10**, 20487 (2018); <https://doi.org/10.1021/acsami.8b04405>

33. H. Gao, X. Zeng, Y. Hu, V. Tileli, L. Li, Y. Ren, X. Meng, F. Maglia, P. Lamp, S.-J. Kim, K. Amine and Z. Chen, *ACS Appl. Energy Mater.*, **1**, 2254 (2018); <https://doi.org/10.1021/acsami.8b00323>
34. J.O. Binder, S.P. Culver, R. Pinedo, D.A. Weber, M.S. Friedrich, K.I. Gries, K. Volz, W.G. Zeier and J. Janek, *ACS Appl. Mater. Interfaces*, **10**, 44452 (2018); <https://doi.org/10.1021/acsami.8b16049>
35. M. Eilers-Rethwisch, S. Hildebrand, M. Evertz, L. Ibing, T. Dagger, M. Winter and F.M. Schappacher, *J. Power Sources*, **397**, 68 (2018); <https://doi.org/10.1016/j.jpowsour.2018.06.072>
36. J.W. Fergus, *J. Power Sources*, **195**, 939 (2010); <https://doi.org/10.1016/j.jpowsour.2009.08.089>
37. C.S. Yoon, K.-J. Park, U.-H. Kim, K.H. Kang, H.-H. Ryu and Y.-K. Sun, *Chem. Mater.*, **29**, 10436 (2017); <https://doi.org/10.1021/acs.chemmater.7b04047>
38. X. Ma, C. Wang, J. Cheng and J. Sun, *Solid State Ion.*, **178**, 125 (2007); <https://doi.org/10.1016/j.ssi.2006.11.017>
39. F. Schipper, M. Dixit, D. Kovacheva, M. Talianker, O. Haik, J. Grinblat, E.M. Erickson, C. Ghanty, D.T. Major, B. Markovsky and D. Aurbach, *J. Mater. Chem. A Mater. Energy Sustain.*, **4**, 16073 (2016); <https://doi.org/10.1039/C6TA06740A>
40. J. Wandt, A.T.S. Freiberg, A. Ogrodnik and H.A. Gasteiger, *Mater. Today*, **21**, 825 (2018); <https://doi.org/10.1016/j.mattod.2018.03.037>
41. M. Dixit, B. Markovsky, F. Schipper, D. Aurbach and D.T. Major, *J. Phys. Chem. C*, **121**, 22628 (2017); <https://doi.org/10.1021/acs.jpcc.7b06122>
42. D.-S. Ko, J.-H. Park, S. Park, Y.N. Ham, S.J. Ahn, J.-H. Park, H.N. Han, E. Lee, W.S. Jeon and C. Jung, *Nano Energy*, **56**, 434 (2019); <https://doi.org/10.1016/j.nanoen.2018.11.046>
43. G. Kang, K. Lee, K. Kwon and J. Song, *Metals (Basel)*, **7**, 395 (2017); <https://doi.org/10.3390/met7100395>
44. J. Li, W. Li, S. Wang, K. Jarvis, J. Yang and A. Manthiram, *Chem. Mater.*, **30**, 3101 (2018); <https://doi.org/10.1021/acs.chemmater.8b01077>
45. J. Yang and Y. Xia, *ACS Appl. Mater. Interfaces*, **8**, 1297 (2016); <https://doi.org/10.1021/acsami.5b09938>